Acta Geotechnica (2023) 18:77–94
https://doi.org/10.1007/s11440-022-01554-0

RESEARCH PAPER

Compressive behavior of kaolinitic clay under chemo-mechanical loadings

Dehuan Yang[1] · Rongtao Yan[1] · Tiantian Ma[2] · Changfu Wei[1,2]

Received: 5 March 2021 / Accepted: 23 March 2022 / Published online: 27 April 2022

Abstract

A series of laboratory experiments, including sedimentation, liquid limit, SEM and oedometer tests, was performed to explore the influence of chemo-mechanical loadings on the compression behavior of kaolinitic clay. The results indicate that the concentration and valence of pore solution have significant effect on the volume change of kaolinitic clay. The volume change can be attributed to the change of intergranular forces caused by the variation of pore water chemistry. It is observed that the recompression curves under mechanical loading after solution replacement at various vertical stresses merge into a single curve. In addition, the salinization-induced volumetric strain under the same vertical stress is independent of the step number of salinization, provided that the total change of ionic strength is the same. A recently developed formulation of intergranular stresses, which accounts for the physicochemical interactions between the solid matrix and the pore solution, is introduced to interpret the experimental results. It is shown that the compression behaviors of kaolinitic clay under complex chemical and mechanical loadings can be remarkably unified by a single intergranular stress, showing the capability of the intergranular stress in describing the chemo-mechanical behavior of kaolinitic clay.

Keywords Chemo-mechanical loadings · Compression behavior · Intergranular stress · Kaolinitic clay

Abbreviations

a_{E}^{α}	Activity of species α in the equilibrium solution
a_{P}^{α}	Activity of species α in the pore solution
c	Molar concentration of equilibrium solution
c_0	Molar concentration of equilibrium solution at the reference state
c^{α}	Molar concentration of species α
c_{E}^{i}	Molar concentration of ionic species i in the equilibrium solution
c_{P}^{i}	Molar concentration of ionic species i in the pore solution
CEC	Cation exchange capacity
c_{fix}	Fixed negative charge density
$c_{\mathrm{fix,e}}$	Effective fixed charge density
e	Void ratio
F	Faraday's constant
G_{s}	Specific gravity of soil
m_{E}^{i}	Molar fraction of ionic species i in the equilibrium solution
m_{P}^{i}	Molar fraction of ionic species i in the pore solution
M^{α}	Molar mass of species α
p_0^{l}	Pressure of pure water at some reference state
p_{E}^{l}	Pressure of the equilibrium solution
p_{P}^{l}	Average pore water pressure
R	Universal gas constant
T	Kelvin temperature
γ_{E}^{i}	Activity coefficient of ionic species i in the equilibrium solution
γ_{P}^{i}	Activity coefficient of ionic species i in the pore solution
δ	Reduction factor
δ_{ij}	Kronecker delta
ε_{v}	Volumetric strain
ξ	Local electrostatic potential
$\mu_{\mathrm{E}}^{\alpha}$	Chemical potential of species α in the equilibrium solution
$\mu_{\mathrm{P}}^{\alpha}$	Chemical potential of species α in the pore solution
$\mu_{\oplus}^{\alpha}$	Chemical potential of species α at the pure state
v	Valence of cation

✉ Changfu Wei
cfwei@whrsm.ac.cn

[1] Guangxi Key Laboratory of Geomechanics and Geotechnical Engineering, Guilin University of Technology, Guilin 541004, Guangxi, China

[2] State Key Laboratory of Geomechanics and Geotechnical Engineering, Institute of Rock and Soil Mechanics, Chinese Academy of Sciences, Wuhan 430071, Hubei, China

v^i	Valence of ionic species i
Π	Generalized osmotic pressure
Π_D	Donnan osmotic pressure
Π_{D0}	Donnan osmotic pressure at the reference state
ρ_d	Dry density of soil
ρ^l	Mass density of the pore solution
$\rho^\alpha_\oplus$	Mass density of species α in pure state
σ_{ij}	Total stress tensor
σ'_{ij}	Terzaghi's effective stress tensor
σ''_{ij}	Intergranular stress tensor
σ'_v	Vertical Terzaghi effective stress
σ''_v	Vertical intergranular stress
τ^S_{ij}	Part of intrinsic skeletal stress
ϕ	Porosity of the sample
ϕ_0	Porosity of the sample at the reference state
Ω^l	Surface force potential
Ω^l_0	Surface force potential at the reference state

1 Introduction

The mechanical behavior of clayey soils is closely related to the chemistry of pore water (or interchangeably, pore solution) due to the existence of the physicochemical interactions between the solid matrix and the pore solution [24]. Increasing engineering activities, such as landfill construction, groundwater extraction, geological disposal of nuclear waste and submarine gas hydrate extraction, may change the pore solution chemistry in soils, and in turn influence their deformation and strength properties [2, 4, 8, 13, 18, 29, 31, 32]. Inadequate design or improper disposal may give rise to serious geotechnical issues or geoenvironmental hazards, such as groundwater pollution, oil production platform collapse and landslides [14, 17, 28, 41]. Therefore, comprehensively understanding the chemo-mechanical properties of clayey soils is of prime importance when the chemo-mechanical loadings come into play.

As one of the most important aspects of soil behavior, the compressibility of clayey soils subjected to various chemical attacks has been attracting research attentions from diverse fields for decades. Bolt [2] studied the compressibility of active clays (mainly montmorillonite) through the oedometer tests on the remolded clay samples prepared by mixing dried powders with solutions of various concentrations, and showed that the compressibility of active clays decreased with the increase of pore fluid concentration, which was in agreement with the double-layer theory. Similar conclusions were drawn on active clay by Mesri and Olson [23], Sridharan and Rao [31], and Di Maio et al. [10]. Barbour and Fredlund [1] suggested that the volumetric deformation, induced by chemical loading, can be generally attributed to two mechanisms, i.e., osmotically induced consolidation and osmotic consolidation. The former is associated with the flow of water molecules driven by osmotic gradient, while the latter is caused by the change of interparticle physicochemical forces. It is believed that the reversibility of the osmotic deformation (i.e., consolidation and swelling) of active clays in response to chemical loading cycles under constant vertical stress depends on the type of salt in pore solution, and the observed mechanical behavior was closely related to the occurrence of ionic exchange in the samples [6, 8, 13, 34].

For non-active clays (say kaolinitic clay, including both pure kaolinite and kaolinitic soil mainly compose of kaolinite), in response to chemo-mechanical interactions, Chen et al. [5] observed that under certain overburden stress (< 300 kPa), the void ratio of kaolinitic clay observably decreased with the increase of cation valence and concentration of salty solution. They suggested that the double-layer theory could be used to account for the influence of cation valence and concentration on compressibility of kaolinitic clay. Di Maio et al. [8–10] found that sodium chloride solutions had negligible effect on the liquid limit, compressibility and residual strength of kaolinitic clay. However, Moore et al. [25] observed that the residual strength increased with the concentrations (from 0.2 to 1.0 g/L) of sodium chloride solutions. Wang and Siu [39] reported that the volume change characteristics of kaolinitic clay samples formed by pore solution with different pH values are significantly different under isotropic confinement. Meanwhile, Wang and Siu [39] also found that the response of kaolinitic clay deformation behavior to sodium chloride solution depended upon the pore solution's pH condition of the prepared samples. They attributed afore-mentioned experimental results to the existence of the highly pH-dependent charges on the edges of particles. These particles would result in different interparticle forces and associated fabrics under various pH conditions. Indeed, the kaolinitic clay sample with a pH value less than the isoelectric point of edge surface (i.e., the pH value at zero zeta potential of the edge sites [38], denoted by IEP_{edge} hereinafter) exhibits opposite behavior compared to that with a pH value lager than IEP_{edge}.

Wahid et al. [36, 37] investigated the chemo-mechanical effects induced by inorganic salt, acid and base solutions on kaolinitic clay, and showed that the physical and mechanical behavior of kaolinitic clay was relatively insensitive to salty solution, but significantly influenced by the pH value. They suggested that the observed mechanical

behavior was probably due to the mineral dissolution (mainly at particle edges) and the change of surface chemistry. The mineral dissolution was observed by Chavali and Ponnapureddy [4] through FT-IR spectra of kaolinitic clay, which was saturated with highly concentrated inorganic acidic solution. Apparently, the afore-mentioned experimental results, which were obtained under specific hydrochemical conditions, were relatively scattering, and no consensus was achieved on the effect of pore solution chemistry on the behavior of kaolinitic clay. Thus far, few efforts have been made to studying the compressibility of kaolinitic clay under various chemo-mechanical loading paths, in spite of its important theoretical and practical relevance, e.g., in evaluating the leakage problem in clay liners or cutoff walls against landfill [5, 19] and analyzing the urban ground subsidence caused by seawater intrusion in coastal areas.

To characterize the influence of pore solution chemistry on the mechanical behavior of clayey soil, some researchers attempted to modify the effective stress equation. Sridharan and Rao [31] proposed an effective stress formula as, $\sigma' = \sigma - p_w^l - (R - A)$, where σ is the external applied stress, p_w^l is the pore water pressure, and $R - A$ represents the interparticle repulsive-minus-attractive stress. The term $R - A$ is used to address the influence of pore solution chemistry on the mechanical behavior of clayey soil. Thus far, a generally accepted expression for $R - A$ is not available. Barbour and Fredlund [1] proposed to adopt the osmotic pressure π as an independent stress state variable to address the osmotic volume change behavior of clayey soil induced by the change of pore solution chemistry. Rao and Thyagaraj [27] developed the total net vertical stress, in which pore fluid osmotic suction component was incorporated, to address the influence of salt solution concentration on the swelling potential of compacted clays.

Wei [40] proposed an effective stress formula, called the intergranular stresses, based on the chemo-mechanical theory of porous media. It has been shown that the proposed intergranular stresses equation can be effectively used to address the water-weakening effect of chalk materials [21] and the swelling behavior of expansive soils [22]. Recently, Tuttolomondo et al. [35] proposed a generalized effective stress for active clay. In this equation, the different structural characteristics of water near clay particles were considered, and the concept of effective density of fixed charge was introduced to characterize the negative charge per unit volume of clay balanced by the non-movable ions of the pore water.

The objective of this paper is twofold: 1) to explore the influence of chemo-mechanical loading paths on the compression behavior of kaolinitic clay based on a series of laboratory experiments, including the sedimentation tests of pore solution with different pH values and the oedometer tests of the water-saturated slurry samples under various chemo-mechanical loading paths; 2) to validate experimentally the applicability of the intergranular stresses proposed by Wei [40] in describing the chemo-mechanical behavior of kaolinitic clay. In the calculations, the effect of the variation of pore water concentration on the intergranular stresses is explicitly characterized.

2 Materials and methods

2.1 Materials

The soil used in this study was a natural clayey soil sampled from Nanning, Guangxi Province, China. To minimize the influence of natural salt and impurity on experimental results, the soil was washed with deionized water (pH = 5.6, electrical conductivity 1.8 μs/cm) for desalination. The salt washing follows the procedure by Wang and Siu [38]. The suspension without electrolyte was firstly dried in an oven at 80 °C for 3–4 days, grinded into powder and then sieved through the 2000-micron sieve. Finally, the treated soil (< 2000-micron) was used for testing. The basic properties are presented in Table 1.

The total specific surface area of soil was measured by the methylene blue method [16, 43], and the cation exchange capacity (CEC) was determined by the barium

Table 1 Physical properties of the tested soil

Soil properties	Unit	Value
Specific gravity, G_s	–	2.73
Total specific surface area	m^2/g	34.42
Cation exchange capacity	meq/100 g	5.49
Consistency limits		
Liquid limit, LL	%	70.36
Plastic limit, PL	%	24.87
Plasticity index, PI	%	45.49
Grain size distribution		
Sand	%	4.37
Silt	%	28.63
Clay	%	67
Mineral composition		
Montmorillonite	%	0
Illite	%	4
Kaolinite	%	60
Quartz	%	31
Hematite	%	5

chloride buffer method [20]. The tested soil is composed of 4.37% sand, 28.63% silt and 67% clay, respectively. The mineralogical composition was determined by X-ray diffraction. The results show that its composition is 4% illite, 60% kaolinite, 31% quartz and 5% hematite, respectively.

The purities, test types, states and suppliers of the chemical reagents (HCl, NaOH, NaCl, $CaCl_2$) used in the experiments are shown in Table 2. The reagents were mixed with deionized water to obtain the desired solutions for the testing programs in the laboratory.

2.2 Experimental procedures

2.2.1 Determination of IEP_{edge}

The mechanical behavior of kaolinitic clay under chemical loading is influenced by the pH value of the pore solution, which is characterized by the value of IEP_{edge}. Here, a series of sedimentation tests under various pH conditions were performed to determine the IEP_{edge} of the tested soil.

In the sedimentation tests, 20 g of dried electrolyte-free soil powder was mixed with the desired chemical solutions to form 100 mL suspension, which was shaken in the 100-mL graduated cylinder. To remove the dissolved gas, all the soil samples were vacuumed for 1 h. Then, the suspension was stirred slowly with a perforated plunger for 100 s. The top of cylinder was sealed with the rubber plug to prevent evaporation. The height of interface between the sediment and the supernatant liquid was recorded once per day. The suspension was considered to reach equilibrium when the height remained constant for 2 $\sim$ 3 days. Usually, the whole process took about 2 $\sim$ 3 weeks. Following the method proposed by Wang and Siu [38], the height of sediment after equilibrium versus pH value was used to characterize the IEP_{edge}. 13 solutions with different pH values (1, 2, 3, 4, 5, 6, 7, 8, 9, 10, 11, 12, and 13, respectively) were used in the experiments. The pH value of the pore solution was adjusted by mixing with HCl, NaOH and deionized water.

Table 2 Analytical reagent

Reagent	Purity	State	Test type	Supplier
HCl	0.36 $\sim$ 0.38	Liquid	ST	Hengyang Kaixin Chemical Co., Ltd
NaOH	$\geq$ 0.96	Solid	ST	
NaCl	$\geq$ 0.995	Solid	LLT and OT	Guangdong Xilong Scientific Co., Ltd
$CaCl_2$	$\geq$ 0.96	Solid	LLT and OT	

ST stands for sedimentation tests, *LLT* stands for liquid limit tests, *OT* stands for oedometer tests

2.2.2 Liquid limit tests

The liquid limits were determined by the cone penetrometer method on the samples mixed with the deionized water, NaCl solutions and $CaCl_2$ solutions with various concentrations. (For both types of solutions, the concentrations were chosen as 0.01, 0.05, 0.1, 0.5, 1.0, 2.0 and 4.0 mol/L, respectively.) In the liquid limit measurement, the mixture of soil and chemical solution was sealed in the air-tight plastic bags and kept in a desiccator for one month to ensure complete hydrate reaction. The water content is equal to the weight of water divided by the weight of dry soil, which can be calculated by subtracting the weight of salt from the dried residual solids (a mixture of dry soil and salt). The amount of salt was calculated by using the volume of water lost during the drying process, the initial salt concentration and the molar mass of the salt.

2.2.3 Chemo-mechanical oedometer tests

To investigate the effect of various chemo-mechanical loading paths on the compressive behavior of the kaolinitic clay, the conventional experimental setup for the oedometer test was modified to incorporate the infiltration of salt solutions as shown in Fig. 1 [13, 24, 42]. By tightening the screws and pressing the O-ring, the gap between the top part, the basement and the cutting ring was sealed to form a closed cavity, so that the fluid flew only through the soil. To resist the corrosiveness of chemical solution, the oedometer cell is made of 304 stainless steel.

A certain amount of the dried electrolytic-free clay powder was mixed with deionized water in a container to form slurry (about 2 times the liquid limit). The slurry was then consolidated under a vertical stress of 20 kPa. In this process, the leachate was collected and the corresponding electrical conductivity was measured to estimate the initial concentration of the pore solution in the prepared sample [27]. When the vertical deformation converged to a steady value (typically it takes 4 days), the consolidated clay was carefully put into a cutting ring with a designated size (61.8 mm diameter and 20 mm height) along the direction of the major principal stress. The moisture content of the samples was about 52%, corresponding saturation was more than 98.5%, at which the soil was considered to be fully saturated. The initial concentration of the pore solution in the prepared samples is summarized in Table 3.

The sample together with the cutting ring was transferred into the oedometer cell (Fig. 1) and then was consolidated again. Once after the deformation of the sample

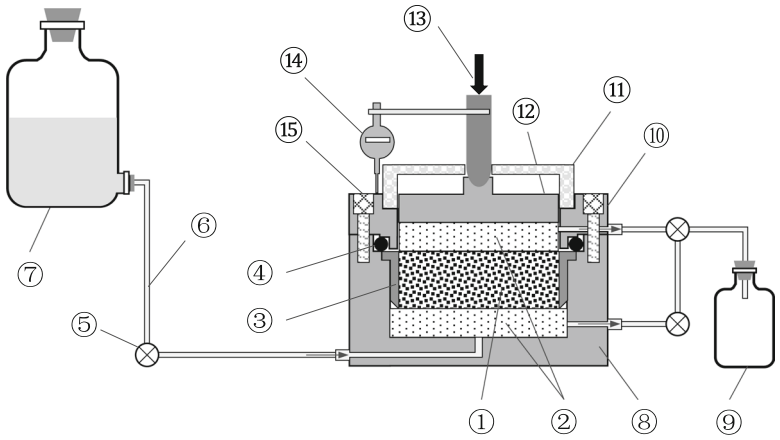

① Sample; ② Porous stones; ③ Cutting ring; ④ O-ring; ⑤ valve; ⑥ Silicone tube; ⑦ Salt solution; ⑧ Basement; ⑨ Liquid collecting bottle; ⑩ Top part; ⑪ Plastic cap; ⑫ Loading Cap; ⑬ Load; ⑭ Strain gauge; ⑮ Screw

Fig. 1 Schematic of modified oedometer testing apparatus

Table 3 Details of the testing conditions used in oedometer tests

Test	Sample No	Initial concentration (mmol/L)	Vertical stresses at replacement (kPa)	Target replacement solution concentration (mol/L)	Solution
Type 1	2, 6, 10, 14	1	50, 100, 200, 800	0.1	NaCl
	3, 7, 11, 15	1	50, 100, 200, 800	0.5	NaCl
	4, 8, 12, 16	1	50, 100, 200, 800	4.0	NaCl
	17, 19	1	50, 200	0.1	$CaCl_2$
	18, 20	1	50, 200	0.5	$CaCl_2$
Type 2	21	1	50	0.1 → 0.5 → 1.0	NaCl
	22	1	200	0.5 → 4.0	NaCl
	23	1	200	0.1 → 0.5 → 4.0	NaCl
Type 3	24	1	50	cyclic chemical loading path (see the footnote)	DW, NaCl, $CaCl_2$
Calibration	1, 5, 9, 13	1	50, 100, 200, 800	0	DW

DW stands for deionized water, whose concentration is assumed to be zero.

The cyclic chemical loading path in Test type 3 was: DW → 1.0 mol/L NaCl → DW → 1.0 mol/L NaCl → 0.5 mol/L $CaCl_2$ → 1.0 mol/L NaCl → DW

under a specified vertical loading converged to a steady value (typically this process took about 1.5 weeks), the chemical loading was carried out. The salt solution went through the bottom porous stone and entered into the samples under the constant vertical stress. During this process, the vertical displacements of the samples were recorded. The vertical deformation was considered to reach a steady state, once the strain rate was less than 0.003 mm within 24 h. After the hydraulic gradient (about 10 kPa) was eliminated and the induced deformation was recorded, the final deformation was obtained. Concentrations of 0.1, 0.5, 1.0, and 4.0 mol/L were selected based on the measurements of the liquid limit (roughly representing the sensitivity of the tested soil to salty solution [18]). The chemo-mechanical loading paths adopted in the experiments are summarized in Table 3.

Three types of chemo-mechanical loading paths were adopted, i.e.,

Type 1 Compression-solution replacement-recompression (CsRR). In these tests, the saturated kaolinitic clay sample was first consolidated up to a specified vertical stress, under which the pore solution was replaced by a salt solution of the targeted concentration, and then mechanically consolidated up to 1000 kPa. The specified vertical stresses under which the pore solution was replaced were chosen as 50, 100, 200, and 800 kPa, respectively.

Type 2 One-step or multi-step salinization. To study the effect of salinization steps on the volumetric strain, the saturated kaolinitic clay samples were first compressed up to a target vertical stress, and then, the concentration of pore solution was changed stepwise to the target value by one step or multiple steps. The targeted vertical stress were chosen as 50 kPa and 200 kPa, respectively.

Type 3 Salinization-desalinization cycle. To identify the potential mechanisms for volume change behavior of clayey soil, a salinization/desalinization test was performed, in which the saturated kaolinitic clay sample was alternatively exposed to different salt solutions (NaCl or $CaCl_2$) and deionized water under a vertical stress of 50 kPa.

2.2.4 Calibration tests

As well known, the infiltration and creeping (that is, the deformation increases with time under constant external mechanical loading after consolidation) would give rise to the sample deformation during the replacement of pore solution in chemo-mechanical oedometer tests [24]. Consequently, the total deformation for chemical loading at constant vertical stress consists of these deformations induced by the pore solution composition change and by the infiltration and creeping. It is assumed that these deformations can be superimposed. To obtain the correct deformation induced by the pore solution composition change, several oedometer tests (denoted by No. 1, 5, 9 and 13, see Table 3) were carried out to evaluate the influence of infiltration and creeping during the chemical loading. In these tests, the vertical stress was applied up to 50 kPa, 100 kPa, 200 kPa and 800 kPa, respectively, and then waited for the same period of time (about 1.5 weeks) before applying chemical loading in the CsRR experiments. The samples were then percolated by the deionized water, and the volumetric strains (i.e., the ratio of the volume change caused by solution replacement to the initial volume of sample) were measured. The percolation time was almost the same as that of replacement salt solution (about 1 month).

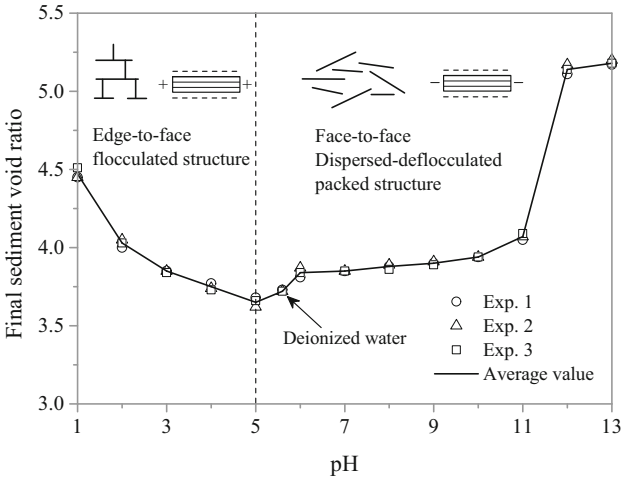

Fig. 2 Final sediment void ratio of kaolinitic clay suspensions as a function of pH value

3 Results and analysis

3.1 Sedimentation tests

Figure 2 presents the final sediment void ratio versus the pH value for kaolinitic clay suspensions. Three parallel experiments were conducted to ensure the repeatability of the experimental results. It can be seen that the final average void ratio of sediment decreased firstly and then increased as the pH value increased. The threshold pH value is approximately equal to 5, at which the clayey soil changes its fabric.

Wang and Siu [38] suggested that at pH < 5, the EF (edge-to-face, see Fig. 2) flocculation occurs due to the Coulombic attraction between oppositely charged edge (positive, due to the protonation) and face (negative), whereas at pH > 5, all the surfaces (edges and faces) are

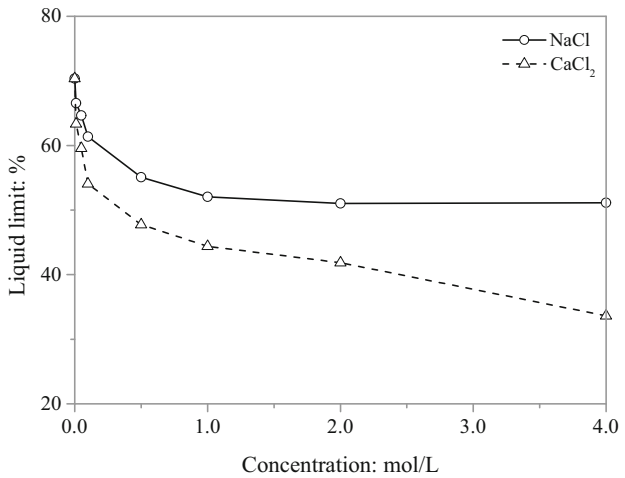

Fig. 3 Effect of salt concentrations on the liquid limit of kaolinitic clay

negatively charged so that the double-layer repulsion becomes dominated, preventing the particles to approach each other and facilitating the formation of the dispersed–deflocculated packed structure (e.g., face-to-face, FF, see Fig. 2). As the pH value decreases (or increases) from the threshold value, the Coulombic attraction (or repulsive energy barrier) between particles is enhanced, resulting in a V-shaped change curve of the sediment void ratio versus the pH value. At the threshold value (pH = 5), the surface charge at the edge site transits between positive and negative, implying that the IEP_{edge} of the tested soil is roughly equal to 5. This result is consistent with the others obtained by the sedimentation test [3, 38]. Although the IEP_{edge} inferred from the sedimentation test is probably not exactly the same as that obtained from the Zeta potential test, as an approximation, an IEP_{edge} of 5 is used here in the subsequent analysis. Indeed, a similar approach was already adopted by Wang and Siu [38].

3.2 Liquid limit tests

Figure 3 shows the relationship between the liquid limit (LL) and the concentrations of NaCl and $CaCl_2$ solutions for kaolinitic clay. It can be seen that the LL decreases significantly with the increase of solution concentration. The influence of $CaCl_2$ solution on LL is more significant than that of NaCl solution, indicating that the testing soil is sensitive to changes in salt solution. These results are consistent with the double-layer theory. Indeed, the increase of the cation concentration or valence may compress the thickness of the double-layers, thereby reducing the water content and the LL. Therefore, the higher the concentration and valence of the cation are, the lower LL is. Remarkably, some researchers also reported that the LL increased with the increasing solution concentration for kaolinitic clay, and they suggested that this phenomenon was due to the EF flocculation of clay particles induced by the reduction of repulsive forces [30, 33, 38]. However, this mechanism does not completely account for the LL change for the kaolinitic clay with relatively large specific surface area unless the response of double-layers thickness is taken into account. As observed by Palomino and Santamarina [26], the high volumetric solid content (referred to the solid volume divided by the total soil volume) hinders EF flocculation, and in this case, the liquid limit depends primarily upon the thickness of the double layer.

Noticeably, our result is inconsistent with the observations by Di Maio et al. [10] and Wahid et al. [36], who showed that the variation of the LL of kaolinitic clay with the concentration of the salt solution was insignificant. The discrepancy is probably due to the fact that the kaolinitic clay used in our study was a natural clayey soil, which had experienced severe physical and chemical weathering and

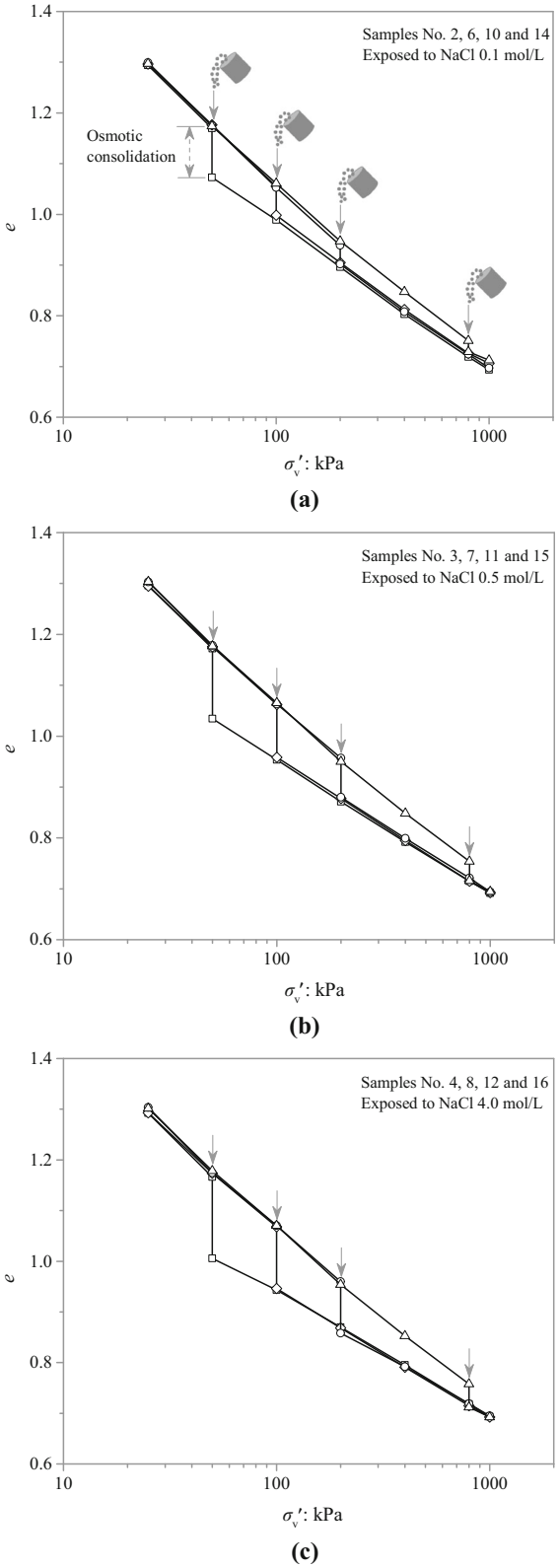

Fig. 4 One-dimensional compression curves of the samples prepared with deionized water and later exposed to a NaCl solution under various vertical stresses (50, 100, 200 and 800 kPa). **a** 0.1 mol/L, **b** 0.5 mol/L, **c** 4.0 mol/L

it contained small amount of illite. Indeed, the kaolinitic clay used in our study has a specific surface area of 34.42 m^2/g (see Table 1), which is much higher than that of the clay used by Wahid et al. [36] ($\sim$ 14 m^2/g), and the clay content ($\sim$ 67%) is also much higher than that used by Di Maio et al. [10] ($\sim$ 30%). Apparently, the kaolinitic clay used in our study is more chemically active than those used in these previous studies.

3.3 Chemo-mechanical oedometer tests

3.3.1 Compression-solution replacement-recompression (CsRR) tests

Figure 4 presents the results of various CsRR oedometer tests for different solution replacements of 0.1, 0.5 and 4.0 mol/L NaCl. Figure 4a shows the void ratio variation of samples with 0.1 mol/L NaCl solution replacement at different specified vertical stresses (50, 100, 200 and 800 kPa, respectively). Apparently, the void ratio of soil decreases first, due to the compaction induced by the applied mechanical loading. Then, at a constant vertical stress, the void ratio decreases due to the chemical loading (i.e., osmotic consolidation). The subsequent mechanical loading further reduces the void ratio. Interestingly, all the recompression curves under further mechanical loading after solution replacement merge into a single one. Similar behavior was observed in the Ponza bentonite by Di Maio [7].

Figure 4b, c shows the variations of void ratio under various chemo-mechanical loadings for the cases of 0.5 and 4.0 mol/L NaCl solution replacement, respectively. The trends of the void ratio variation are similar to those of 0.1 mol/L NaCl solution replacement. Nevertheless, it is clear that under the same vertical stress, the void ratio variation induced by solution replacement is more significant, if the concentration of the replacement solution is higher for the case of samples prepared with deionized water. For more comparison of volumetric strain changes (hereinafter referred to as the osmotic volumetric strain) caused by chemical loading under constant vertical stress, see later.

Figure 5 presents the results of various CsRR oedometer tests for different solution replacements of 0.1 and 0.5 mol/L $CaCl_2$. As can be seen from the figure, similar to the replacement of NaCl solution, the significant decrease of void ratio caused by chemical loading was observed. In addition, once after the solution replacement is completed, all the compression curves resulting from further mechanical loading at the same concentration practically merge into a single curve. Based on these experimental results, it can be inferred that for slurry remolding kaolinitic clay samples, the recompression curves under the mechanical loading after the same solution replacement are independent of the chemo-mechanical loading paths.

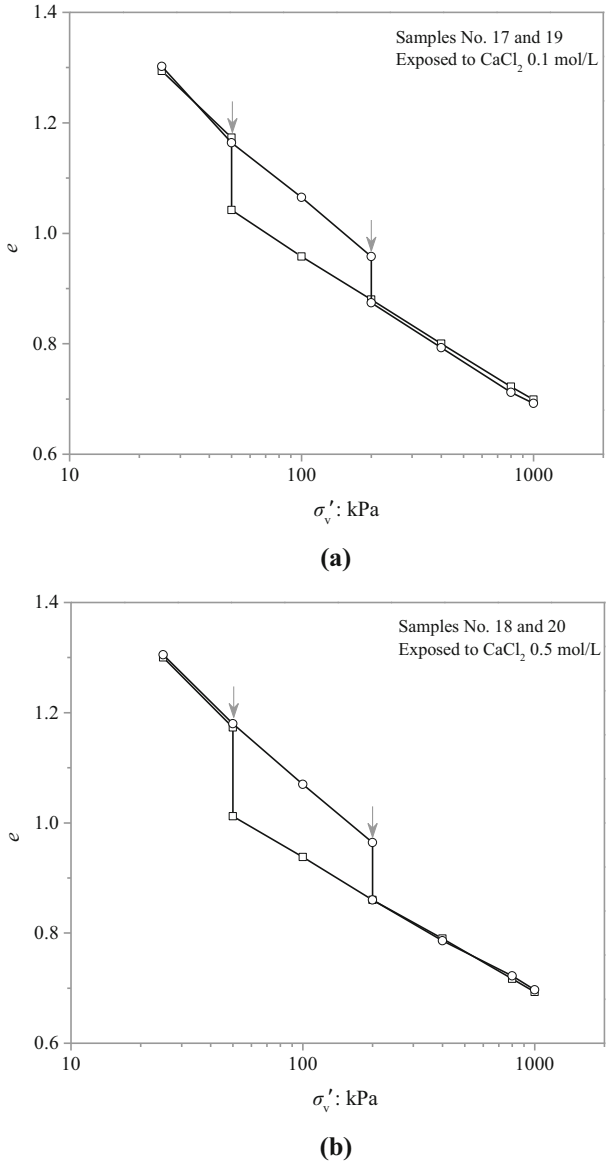

Fig. 5 One-dimensional compression curves of the samples prepared with deionized water and later exposed to a CaCl2 solution under various vertical stresses (50 and 200 kPa). **a** 0.1 mol/L, **b** 0.5 mol/L

Combining the results in Figs. 4 and 5, the total osmotic volumetric strain induced by pore solutions containing various salts (NaCl or $CaCl_2$) at different vertical stresses was reprocessed, as shown in Fig. 6. It can be seen that the osmotic volumetric strain decreases monotonically with increasing the applied vertical stress at the same replacement solution (including concentration and composition). In addition, for the same salt and the same vertical stress, the osmotic volumetric strain increases monotonically with increasing replacement solution concentration under the experimental conditions here.

In Fig. 6, one can find the volumetric strain responses of samples to NaCl solution and $CaCl_2$ solution at 50 kPa and 200 kPa vertical stresses. It is clear that the osmotic volumetric strain induced by 0.5 mol/L $CaCl_2$ solution (6.62%) is greater than that of 4.0 mol/L NaCl solution (6.57%) under the vertical stress of 50 kPa. Although the absolute value of osmotic volumetric strain decreases with increasing vertical stress, a similar trend can be observed at the vertical stress of 200 kPa. This indicates that the effect of $CaCl_2$ solution on the osmotic volumetric strain is more significant than that of NaCl solution, implying that the effect of ionic valence on the osmotic volumetric strain is more pronounced compared to that of concentration for the species and concentrations considered here. The trend of variation of volumetric strain in osmotic consolidation is roughly consistent with the variation of the liquid limit with solution concentration (see Fig. 3), implying that similar physicochemical mechanisms are functioning at the place.

Remarkably, Di Maio et al. [7, 10] and Wahid et al. [37] showed that inorganic salt solution has negligible effects on the compression behavior for kaolinitic clay. This is inconsistent with our results presented here. As pointed out above, the reason is that the kaolinitic clay used in this study is more chemically active than those used in the previous studies.

Figure 6 also includes the results of calibration tests, which are about the variations of volumetric strain induced by deionized water. It can be seen that the variations of volumetric strain induced by deionized water are 0.09%, 0.06%, 0.04% and 0.02% under the constant vertical stresses of 50 kPa, 100 kPa, 200 kPa and 800 kPa, respectively. Compared to the osmotic volumetric strain

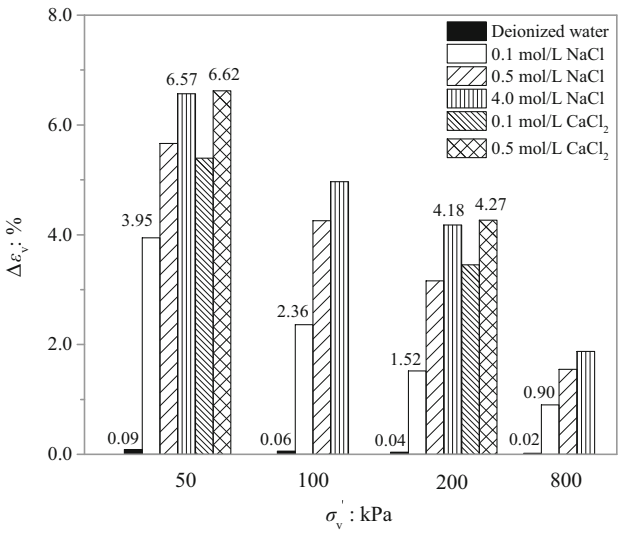

Fig. 6 Variation of volumetric strain with concentrations of the replacement solution under different vertical stresses

caused by salt solution (see Fig. 6), the change of volumetric strain due to infiltration and creeping is very small so that it can be neglected. That is, in the experiment performed here, the deformation induced by chemical loading is mainly due to the change of the pore solution composition. Considering the small contribution of infiltration and creeping to deformation during chemical loading, the osmotic volumetric strain obtained in this test is not modified.

The deformation behavior of soil depends largely on the evolution of intergranular forces and soil microfabric [24]. To clarify the changes of soil microfabric during chemo-mechanical loading, the SEM tests were performed on samples with different states, as shown in Fig. 7. These oedometer tests were independently performed on the parallel samples and are not listed in Table 3. To minimize the effect of fabric changes due to unloading and capillary effects, the tested samples were rapidly placed in the liquid nitrogen, after deposition or consolidation, to quickly freeze its pore water [38].

Figure 7a presents the SEM image of the sample (i.e., the sediment) after deposition in deionized water without loading. It can be seen that, except for a few edge-to-face (EF) flocculation, the particles are oriented approximately in the same direction, representing face-to-face (FF) aggregation. This is consistent with the result inferred from the sedimentation test. During mechanical loading, the previous fabric feature (i.e., FF aggregation) of the sediment was preserved in the samples (Fig. 7b, c). During chemical loading, the sample was exposed to the salt solution under a vertical stress of 50 kPa until it reached a steady state, at which the FF aggregated fabric was readily seen in the samples with different solutions (Fig. 7d, e and f). These SEM images indicate that the main features (FF aggregation) of the fabric of kaolinitic clay formed in the deposition stage were reserved in subsequent mechanical and chemical loadings. This can be attributed to the fact that the packed FF alignment is a type of stable fabrics, which can limit the steering and rolling of particles [39].

The similarity between the microfabric changes induced by chemical and mechanical loadings implies that the deformation induced by these two types of loadings is induced by similar mechanisms, namely, the change of effective stress. At a constant vertical stress, the double-layer repulsion is weakened by the infiltration of electrolyte solution, and thus the net attraction force between particles is enhanced (i.e., the effective stress increases), resulting in soil compression (or osmotic consolidation). Because the change of the thickness of diffuse double layer is proportional to the solution concentration or cationic valence [1, 15, 24], the higher the concentration or cationic valence of the replacement solution, the greater the corresponding osmotic volumetric strain for the samples prepared with

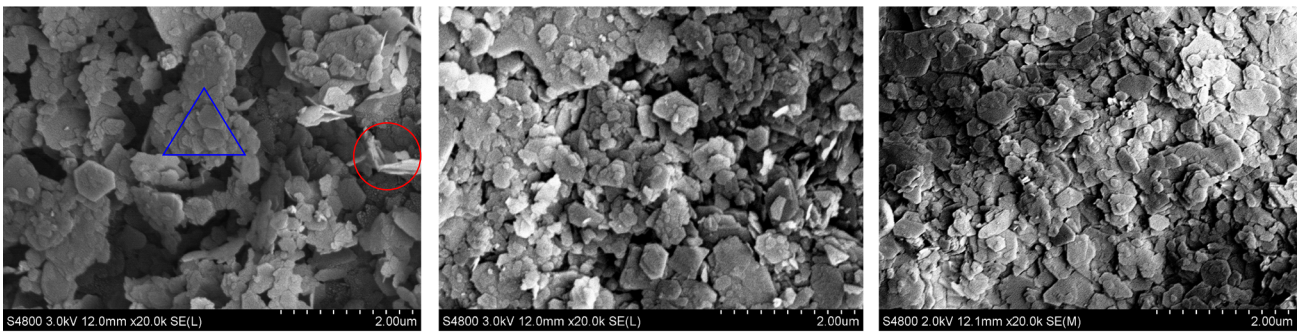

(a) Deionized water (0 kPa) **(b)** Deionized water (50 kPa) **(c)** Deionized water (1000 kPa)

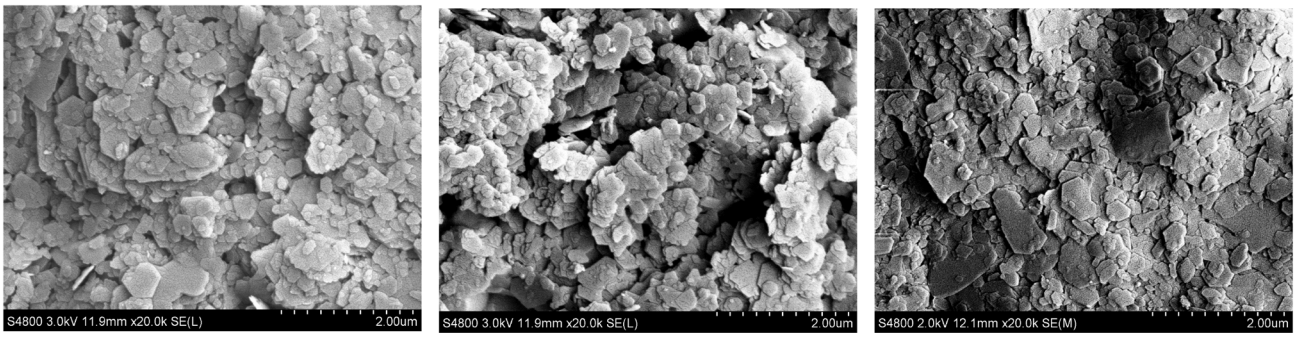

(d) 0.1 mol/L NaCl (50 kPa) **(e)** 4.0 mol/L NaCl (50 kPa) **(f)** 0.1 mol/L $CaCl_2$ (50 kPa)

Fig. 7 SEM images of the samples under a vertical stress of 50 kPa. ○, edge-to-face flocculation; △, face-to-face aggregation

deionized water. Under larger mechanical loading, the soil becomes denser and the deformation resistance between particles becomes stronger, so that less deformation is induced by chemical loading.

3.3.2 One-step or multi-step salinization tests

Figure 8 shows the results of volumetric strain changes induced by one-step and multi-step chemical loadings under constant vertical stresses of 50 kPa and 200 kPa, respectively. Figure 8a shows the volumetric strain for mechanical loading from 25 to 50 kPa, and the volumetric strain for chemical loading at constant vertical stress of 50 kPa. In one-step chemical loading (No. 24), the induced volumetric strain is 6.19%, which is practically equal to that under multi-step chemical loading (No. 21), which is 6.08%. Similar tests were conducted under 200 kPa constant vertical stress with three different salinization schemes (No. 16, 22, and 23), and the experimental results are shown in Fig. 8b. The change of volumetric strains induced by chemical loading are 4.18%, 4.18% and 4.10% for No. 16, No. 22, and No. 23, respectively. These results clearly indicate that the step number of salinization has a negligible effect on the osmotic volumetric strain of kaolinitic clay samples within the experimental time scale. Noticeably, Fig. 8a illustrates that the temporal variation of ε_v shows a sudden drop by the end of the salinization. This can be attributed to the elimination of the hydraulic gradient (about 10 kPa) that drives the salt solution into the sample, resulting in an increase in the effective stress. Such a sudden increase of ε_v does not appear significantly at the vertical stress of 200 kPa (Fig. 8b), since the soil sample is denser under a larger vertical stress, and the volumetric strain induced by the elimination of the hydraulic gradient is less pronounced.

3.3.3 Salinization-desalinization cycle tests

Figure 9 shows the development of the volumetric strain of the sample subjected to cyclic exposures to different salt solutions (NaCl or $CaCl_2$) and deionized water, under the vertical stress of 50 kPa.

Figure 9b is the enlargement of the local variation of volumetric strain during cyclic loading (Fig. 9a). Clearly, when the sample previously exposed to NaCl solution was re-exposed to deionized water (i.e., BC), the recovered volumetric strain (osmotic swelling) due to desalinization was very small, compared to the volumetric strain induced by the previous chemical loading (i.e., AB). This implies that chemically induced volumetric compression is irreversible for the kaolinitic clay. However, when the kaolinitic clay sample was again exposed to a NaCl solution (i.e., CD), the volumetric strain was compressed to almost the same value as the first salinization (i.e., point B), implying that the osmotic swelling in BC is reversible, and associated with the change of the double layer thickness in

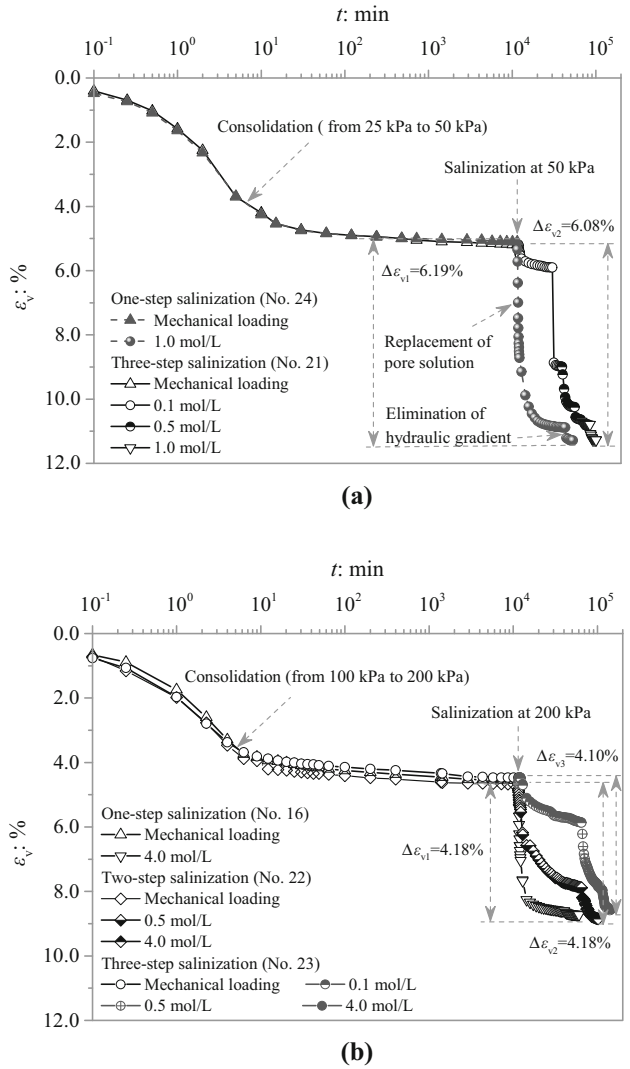

Fig. 8 Effect of the salinization steps on the osmotic volumetric strain

the desalinization phase [8]. The above experimental results clearly indicate that the osmotic (irreversible) volumetric strain of kaolinitic clay is mainly due to the particle rearrangement governed by intergranular forces, rather than the compression of the diffuse double layers which results in reversible deformation.

From D to E, the 1.0 mol/L NaCl solution was replaced by the 0.5 mol/L $CaCl_2$ solution, and then from E to F, the 0.5 mol/L $CaCl_2$ solution was again replaced by the 1.0 mol/L NaCl solution. Noticeably, these two solutions have the same amount of cationic charges but different valences. By comparing the osmotic volumetric strains in DE and EF, it is clear that about 0.10% of the osmotic volumetric strains were produced when Na^+ was replaced by Ca^{2+} in the solution. Finally, from F to G, the kaolinitic clay sample was re-exposed to deionized water, and the soil sample swelled to some extent until equilibrium was reached at point G. Interestingly, from C to G, the volumetric strain increased by 0.15%, which is very close to the amount induced by the replacement of the 1.0 mol/L NaCl solution with the 0.5 mol/L $CaCl_2$ solution (i.e., 0.10% from D to E). Hence, it is suggested here that the replacement of Na^+ with Ca^{2+} in pore solution may induce a slight increase of intergranular forces, resulting in particle rearrangement and irreversible skeletal deformation.

4 Theoretical characterization

4.1 Intergranular stress

Traditionally, Terzaghi's effective stresses have been used as stress state variables to characterize the mechanical behavior of fluid-saturated soils. Terzaghi's effective stress tensor, σ'_{ij}, can be written as $\sigma'_{ij} = \sigma_{ij} - u_w\delta_{ij}$, where σ_{ij} is

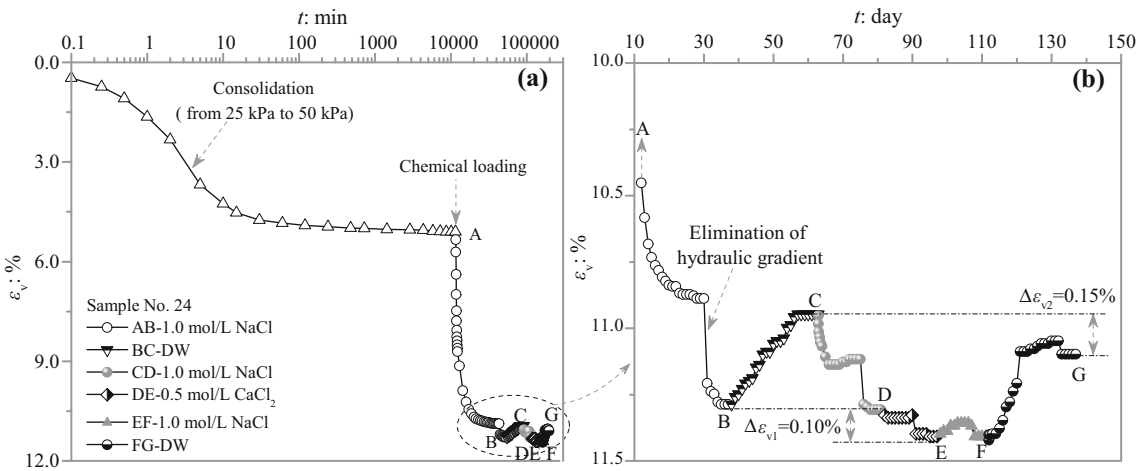

Fig. 9 Evolution of volumetric strain of kaolinitic clay during cyclic exposure to the different salt solutions under the vertical stress of 50 kPa

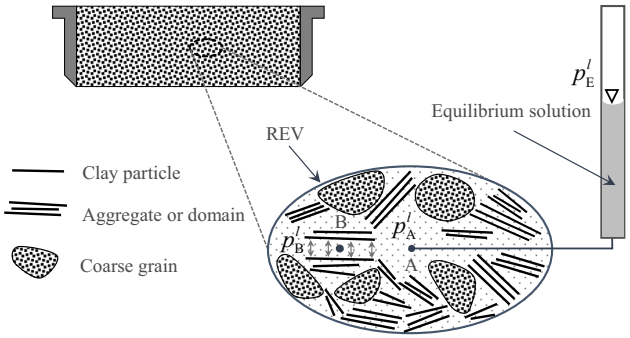

Fig. 10 Schematic illustration of saturated soil–water system. Due to the physicochemical interactions between solid grains and pore solution, local pore water pressure is heterogeneously distributed over the representative elementary volume (REV), particularly, $p_A^l \neq p_B^l$. In the pore water pressure measurement, what is measured is indeed the pressure of the equilibrium solution (p_E^l)

the total stress tensor, u_w is the pore water pressure and equal to the pressure of a *virtual* equilibrium solution (denoted by p_E^l hereinafter) [22], and δ_{ij} is the Kronecker delta. The equilibrium solution is defined as the water solution in the reservoir (Fig. 10) that is hydraulically connected and equilibrated with the pore water in the soil. It has been well recognized that Terzaghi's effective stress is insufficient to describe the behavior of clayey soils [24, 31]. Indeed, due to the long-range interactions between solid grains and pore water, *local* distribution of the pore water pressure in clayey soils is generally heterogeneous [15], as schematically shown in Fig. 10. In particular, the water pressure in the vicinity of grain contacts (say at Point B) is different from those far away from grain surfaces (say at Point A). Hence, u_w in Terzaghi's effective stresses does not take into account the effect of the local heterogeneous distribution of pore water pressure stemming from clay–water interactions.

To resolve this problem, Wei [40] proposed the concept of intergranular stresses, based on the continuum theory of porous media, as a substitute for Terzaghi's effective stresses to address the chemo-mechanical behavior of soils. The intergranular stress tensor proposed by Wei [40] has two unique features, i.e., it is transferred through grain contacts, while work-conjugated with the skeletal strains. Explicitly, the proposed intergranular stress tensor (σ_{ij}'') is given by

$$\sigma_{ij}'' = (1-\phi)\tau_{ij}^S = \sigma_{ij}' - \phi\,\Pi\delta_{ij} \tag{1}$$

where ϕ is the porosity, τ_{ij}^S is the part of *intrinsic* skeletal stresses that is transferred through grain contacts, Π ($= p_{\mathrm{P}}^l - p_{\mathrm{E}}^l$) is the generalized osmotic pressure, accounting for the effect of physicochemical interactions between the solid matrix and the pore fluid, and p_{P}^l is the *average* pore water pressure (over the pore space). It can be proved that (Appendix 1)

$$\Pi = \Pi_{\mathrm{D}} - \rho_{\oplus}^{\mathrm{H_2O}}\Omega^l \tag{2}$$

where Π_{D} is the Donnan's osmotic pressure, associated with the electrically charged nature of the soil; $\rho_{\oplus}^{\mathrm{H_2O}}$ is the mass density of the pure water (1.0 g/cm^3), and Ω^l is the surface force potential. Apparently, $-\rho_{\oplus}^{\mathrm{H_2O}}\Omega^l$ represents the contribution of the surfaces forces induced by the interactions between the solid matrix and the pore fluid.

Donnan's osmotic pressure is given by

$$\Pi_{\mathrm{D}} = \frac{RT\rho_{\oplus}^{\mathrm{H_2O}}}{\mathrm{M}^{\mathrm{H_2O}}}\ln\left(\frac{a_{\mathrm{E}}^{\mathrm{H_2O}}}{a_{\mathrm{P}}^{\mathrm{H_2O}}}\right) \tag{3}$$

where R is the universal gas constant and equal to 8.314 J/(mol·K), T is the absolute temperature (K), $\mathrm{M}^{\mathrm{H_2O}}$ is the molar mass of water (18 g/mol), $a_{\mathrm{P}}^{\mathrm{H_2O}}$ and $a_{\mathrm{E}}^{\mathrm{H_2O}}$ are the water activities in the pore water and the equilibrium solution, respectively.

In general, Ω^l is a function of porosity ϕ, the concentration of the equilibrium solution c and the fixed charge density of soil c_{fix}. At full saturation, matric suction vanishes, and one has [40]

$$\phi\rho^l\Omega^l = \phi_0\rho_{\oplus}^{\mathrm{H_2O}}\Omega_0^l + \int_{\phi}^{\phi_0}\Pi_{\mathrm{D}}\mathrm{d}\phi \tag{4}$$

where subscript "0" refers to the initial (reference) state, ρ^l is the mass density of the pore solution. Noticeably, for dilute solution, ρ^l is approximately equal to $\rho_{\oplus}^{\mathrm{H_2O}}$, and thus $\rho_{\oplus}^{\mathrm{H_2O}}$ and ρ^l are used interchangeably in this paper.

4.2 Applicability of intergranular stress as effective stress

Clearly, the intergranular stress tensor σ_{ij}'' has two independent contributions, i.e., a purely mechanical contribution, represented by Terzaghi's effective stresses σ_{ij}', and a physicochemical one, given by $-\phi\,\Pi$. With the two unique features stated above, σ_{ij}'' should be capable of describing the mechanical behavior of clayey soils as the effective stresses. To demonstrate this, the results of oedometer tests in Figs. 4 and 5 are recast onto the $\sigma_{\mathrm{v}}'' \sim e$ plane, where σ_{v}'' is the vertical of the intergranular stresses. Here the working hypothesis is that the physicochemical component of σ_{ij}'' induces skeletal deformation just in the same way as its mechanical counterpart does, and thus, all the data points in Fig. 4 (or 5) should converge into a single smooth curve on the $\sigma_{\mathrm{v}}'' \sim e$ plane, as schematically shown in Fig. 11.

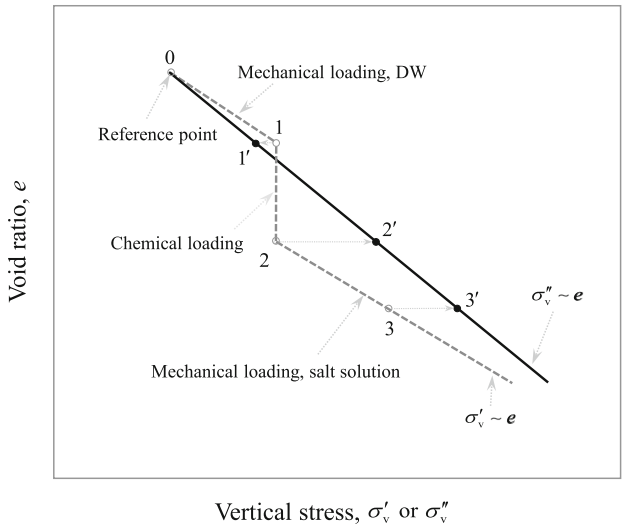

Fig. 11 Schematics of compression curves in different coordinate systems. When casted on the $\sigma_v'' \sim e$ plane, the compression curves converge into a single curve

To evaluate σ_v'', one has to determine Π_D and Ω_0^l first. Π_D is determined by Eq. (3) with given ϕ, c_{fix} and c, and explicitly given in Appendix 1. Noticeably, the value of Ω_0^l in Eq. (4) is generally unknown. However, existence of nonzero Ω_0^l can simply be considered as the physical origin of the initial stress of soil at the initial state. Equation (1) implies that the initial intergranular stress is given by $\sigma_{v0}'' = \sigma_{v0}' + \phi_0 \rho_{\oplus}^{H_2O} \Omega_0^l - \phi_0 \Pi_{D0}$, which holds the soil intact. In this paper, all the samples were consolidated with a vertical stress of 20 kPa and then unloaded to 0 kPa. Hence, at the initial state, σ_{v0}'=0 kPa and $\sigma_{v0}'' = \phi_0 \rho_{\oplus}^{H_2O} \Omega_0^l - \phi_0 \Pi_{D0}$. In the following, unless otherwise explicitly specified, σ_v'' is used to replace $\sigma_v'' - \sigma_{v0}''$ for convenience.

To evaluate Π_{D0}, it is also necessary to determine the concentration of equilibrium solution at the initial state (denoted by c_0). In this paper, the leachate collected during sample preparation was used as the equilibrium solution at the initial state. By the electrical conductivity method [27], c_0 was determined as 1 mmol/L, which corresponds to an electrical conductivity of 138.8 us/cm (of equilibrium solution). With these conditions, σ_v'' can be evaluated for any chemical and mechanical loading paths (Appendix 2). In calculation, the pore solution is considered as an ideal dilute solution. In general, the NaCl solution can be considered as an ideal solution over a wide range of concentration [44]. For the $CaCl_2$ solution, the concentration adopted in our test is relatively small. Hence, as a first approximation, it is assumed here that all the solutions are ideal in the calculation. In addition, the reduction factor δ of the CEC is determined by fitting the calculated results with experimental data, and approximately equal to 0.5.

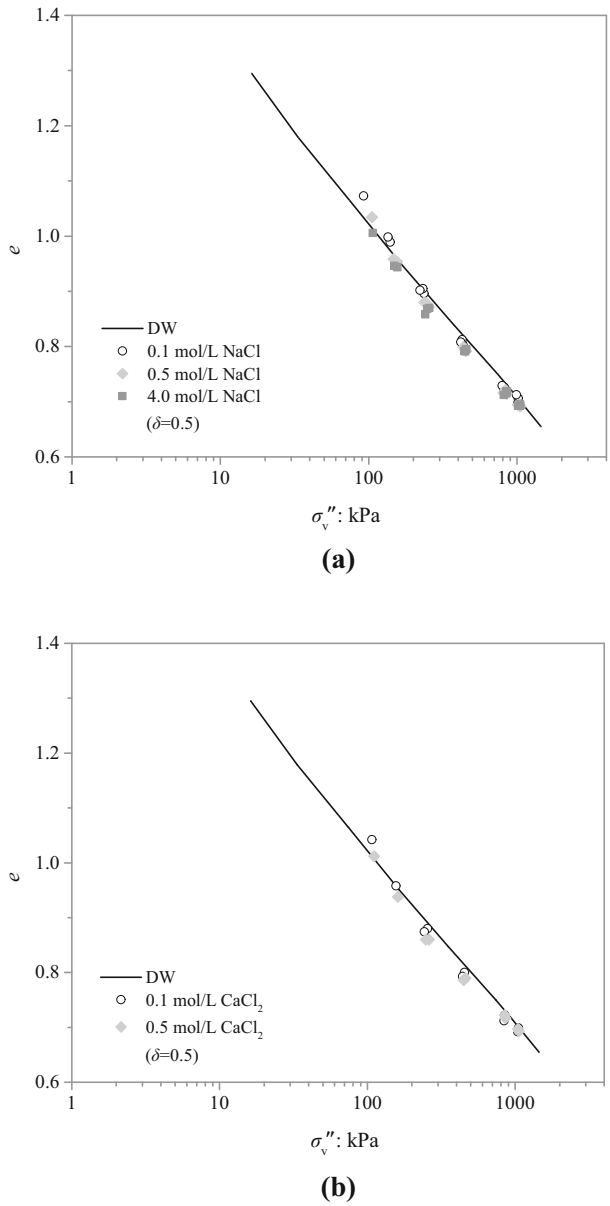

Fig. 12 The calculated $\sigma_v'' - e$ relationships for the samples prepared with deionized water and later exposed to salt solution under various vertical stresses: **a** NaCl solution-saturated; **b** $CaCl_2$ solution-saturated

Figure 12 presents the calculated results of various CsRR oedometer tests on the samples exposed to NaCl solution and $CaCl_2$ solution, onto the $\sigma_v'' \sim e$ plane. For comparison, the compression curve (the solid curve) of the sample saturated with deionized water is also given. Apparently, for both types of samples, which were exposed to NaCl and $CaCl_2$ solutions, respectively, all the experimental points converge into a small vicinity of the compression curve of the sample saturated with deionized water, showing that both chemical and mechanical loadings

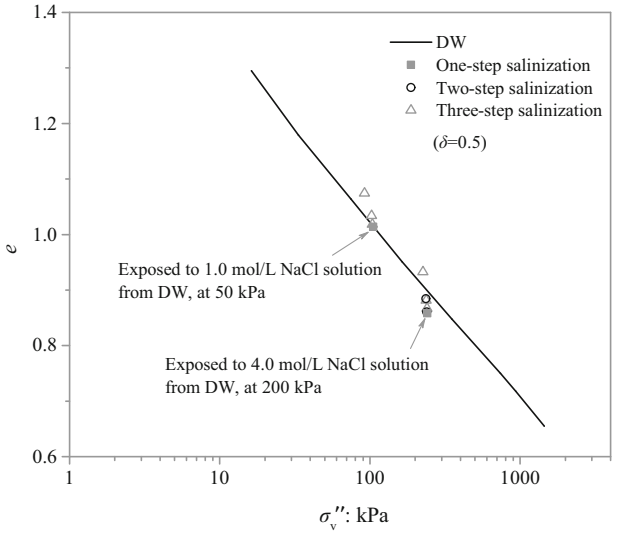

Fig. 13 The $\sigma_v'' - e$ relationship in one-step or multi-step salinization experiments under various vertical stresses (50 and 200 kPa)

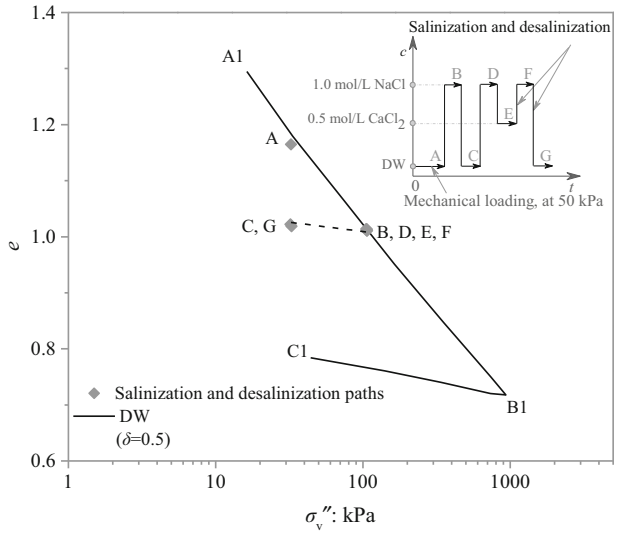

Fig. 14 The $\sigma_v'' - e$ relationship in salinization-desalinization cycle experiments under the vertical stress of 50 kPa

can be reasonably described by a unique intergranular stress formula.

Figure 13 shows the experimental results, which are recast onto the $\sigma_v'' - e$ plane, of the samples prepared with deionized water and later exposed to NaCl solution under the vertical stresses (50 and 200 kPa, respectively) in one-step or multi-step salinization (Type 2 in Table 3). Apparently, all the experimental points also converge into a small vicinity of the compression curve of the sample saturated with deionized water, again showing that the intergranular stress can be used to unify the behaviors of kaolinitic clay under chemical and mechanical loadings.

Figure 14 depicts the $\sigma_v'' - e$ relationships of the sample initially prepared with deionized water under a vertical stress of 50 kPa in the salinization-desalinization cycle experiments (Type 3 in Table 3). For comparison, the mechanical loading and unloading curves (denoted by A1-B1-C1) for the sample saturated by the deionized water are also presented. The experimental procedure is schematically illustrated in the right upper part of the figure. From A to G, three salinization and desalinization cycles were performed: from A to C, the deionized water-saturated sample was first exposed to a 1.0 mol/L NaCl solution (salinized), and then desalinized; from C to D, the sample was salinized again by a 1.0 mol/L NaCl solution and then desalinized from D to E, where the saturating 1.0 mol/L NaCl solution was replaced by a 0.5 mol/L $CaCl_2$ solution; finally, from E to F, the saturating 0.5 $CaCl_2$ solution was replaced by a 1.0 mol/L NaCl solution and then desalinized from F to G. Clearly, the first salinization (from A to B) is a chemical loading process, and the compression practically follows the virgin compression curve. The following desalinization (from B to C) represents chemical unloading, while the re-salinization (from C to D) is chemical reloading. It can be seen that the B-C and C-D curves (i.e., dashed curve) are approximately parallel to the unloading-reloading curve (B1-C1), implying that the rebound index is independent of the applied vertical stress and solution concentration.

From D to E, the 1.0 mol/L NaCl solution was replaced by 0.5 mol/L $CaCl_2$. In the process, the type of salt solution was changed, though the amount of cationic charges remained the same, and the induced volumetric strain is very small (about 0.1%). This implies that the volumetric strain is mainly due to the change of ionic strength (i.e., induced intergranular stress) but the type of salt. Similarly, from E to F, the 0.5 mol/L $CaCl_2$ solution was replaced by the 1.0 mol/L NaCl solution, the intergranular stress remained practically unchanged, and thus no significant deformation occurred. Based on the above results, it is concluded that the chemo-mechanical behavior of kaolinitic clay can be very well described by the intergranular stress.

5 Conclusion

A series of experiments, including sedimentation tests, liquid limit tests, SEM tests and oedometer tests, on the remolded kaolinitic clay was performed under various chemo-mechanical loadings. It is shown that the concentration and valence of pore solution have significant effect on the volume change of kaolinitic clay. The volume change can be attributed to the change of intergranular forces caused by the variation of pore water chemistry. In addition, in the compression-solution replacement-

recompression tests, all the recompression curves under the subsequent mechanical loading after solution replacement merge into a single curve, provided that the replacing solution is the same. If the change of ionic strength is the same, the induced osmotic volumetric strain is independent of the step number of salinization. The results of sedimentation tests imply that clay mineral face-to-face (FF) aggregation prevails in the soil sample. The SEM-based microstructural analysis reveals that such a FF-aggregation fabric remains practically unchanged during both mechanical and chemical loadings.

The concept of intergranular stress by Wei [40] is introduced to interpret the experimental results, and a simple procedure is provided to calculate the intergranular stress. It is found that when Terzaghi's effective stress is replaced by the introduced intergranular stress, the compression curves under various chemo-mechanical loadings converge into a small vicinity of the compression curve of the deionized water-saturated sample. This result implies that the behaviors of kaolinitic clay under complex chemical and mechanical loadings can be remarkably unified by a single intergranular stress. Nonetheless, further research needs to be pursued to explore the applicability of the intergranular stress equation for other soils, especially highly active clay, say montmorillonite.

Appendix

Determination of osmotic pressures Π and Π_D

The detailed derivations can be found in Wei [40], and for easy reference are also presented here. Both NaCl and $CaCl_2$ solutions are of concern here. For clarity, both solutions can be denoted by BA_v, where B^{v+} represents the cations with a valence of v, and A^- the monovalent anions. When the system in Fig. 10 is in equilibrium, for any species α (= H_2O, B^{v+} or A^-), one has

$$\mu_{\mathrm{E}}^{\alpha} = \mu_{\mathrm{P}}^{\alpha} \tag{A.1}$$

where $\mu_{\mathrm{E}}^{\alpha}$ and $\mu_{\mathrm{P}}^{\alpha}$ are the chemical potentials of species α in the equilibrium solution and in the pore water in the soil, respectively. In the equilibrium solution,

$$\mu_{\mathrm{E}}^{\mathrm{H_2O}} = \mu_{\oplus}^{\mathrm{H_2O}}(T, p_0^l) + \frac{(p_{\mathrm{E}}^l - p_0^l)}{\rho_{\oplus}^{\mathrm{H_2O}}} + \frac{\mathrm{RT}}{\mathrm{M}^{\mathrm{H_2O}}} \ln a_{\mathrm{E}}^{\mathrm{H_2O}} \tag{A.2}$$

$$\mu_{\mathrm{E}}^{i} = \mu_{\oplus}^{i}(T, p_0^l) + \frac{(p_{\mathrm{E}}^l - p_0^l)}{\rho_{\oplus}^{i}} + \frac{\mathrm{RT}}{\mathrm{M}^{i}} \ln a_{\mathrm{E}}^{i} + \frac{F\xi v^i}{\mathrm{M}^{i}} \quad (i = \mathrm{B}^{v+} \text{or } \mathrm{A}^-) \tag{A.3}$$

In the pore space,

$$\mu_{\mathrm{P}}^{\mathrm{H_2O}} = \mu_{\oplus}^{\mathrm{H_2O}}(T, p_0^l) + \frac{(p_{\mathrm{P}}^l - p_0^l)}{\rho_{\oplus}^{\mathrm{H_2O}}} + \frac{\mathrm{RT}}{\mathrm{M}^{\mathrm{H_2O}}} \ln a_{\mathrm{P}}^{\mathrm{H_2O}} + \Omega^l \tag{A.4}$$

$$\mu_{\mathrm{P}}^{i} = \mu_{\oplus}^{i}(T, p_0^l) + \frac{(p_{\mathrm{P}}^l - p_0^l)}{\rho_{\oplus}^{i}} + \frac{\mathrm{RT}}{\mathrm{M}^{i}} \ln a_{\mathrm{P}}^{i} + \Omega^l + \frac{F\xi v^i}{\mathrm{M}^{i}} \quad (i = \mathrm{B}^{v+} \text{or } \mathrm{A}^-) \tag{A.5}$$

where $\mu_{\oplus}^{\alpha}$ is the chemical potential of species α in its pure state (i.e., pure substance), depending only upon T and p; $\rho_{\oplus}^{\alpha}$ the mass density of species α at the pure state; F Faraday's constant; ξ the local electrostatic potential; v^i the valence of ionic species i; M^{α} the molar mass of species α; a_{E}^{i} the activity of ionic species i in the equilibrium solution; a_{P}^{i} the activity of ionic species i in the pore solution.

Applying Eq. (A.1) to the solvent (i.e., H_2O), i.e., $\mu_{\mathrm{E}}^{\mathrm{H_2O}} = \mu_{\mathrm{P}}^{\mathrm{H_2O}}$, and combining Eqs. (A.2) and (A.4), one obtains

$$\Pi = p_{\mathrm{P}}^l - p_{\mathrm{E}}^l = \frac{\mathrm{RT}\rho_{\oplus}^{\mathrm{H_2O}}}{\mathrm{M}^{\mathrm{H_2O}}} \ln\left(\frac{a_{\mathrm{E}}^{\mathrm{H_2O}}}{a_{\mathrm{P}}^{\mathrm{H_2O}}}\right) - \rho_{\oplus}^{\mathrm{H_2O}}\Omega^l \tag{A.6}$$

The firsts term on the right of the second equation is Donnan's osmotic pressure, Π_{D}, given by Eq. (3). Now Eq. (2) immediately follows after substituting Π_{D} in Eq. (A.6).

Applying Eq. (A.1) to both ionic species (i.e., B^{v+} and A^-), i.e., $\mu_{\mathrm{E}}^{\mathrm{B}^{v+}} = \mu_{\mathrm{P}}^{\mathrm{B}^{v+}}$ and $\mu_{\mathrm{E}}^{\mathrm{A}^-} = \mu_{\mathrm{P}}^{\mathrm{A}^-}$, one can derive

$$\mu_{\mathrm{E}}^{\mathrm{B}^{v+}} + v\mu_{\mathrm{E}}^{\mathrm{A}^-} = \mu_{\mathrm{P}}^{\mathrm{B}^{v+}} + v\mu_{\mathrm{P}}^{\mathrm{A}^-} \tag{A.7}$$

By substituting Eqs. (A.3) and (A.5) in Eq. (A.7), one can derive

$$\ln\left[a_{\mathrm{P}}^{\mathrm{B}^{v+}}\left(a_{\mathrm{P}}^{\mathrm{A}^-}\right)^v\right] = \ln\left[a_{\mathrm{E}}^{\mathrm{B}^{v+}}\left(a_{\mathrm{E}}^{\mathrm{A}^-}\right)^v\right] + O(\varepsilon) \tag{A.8}$$

where $O(\varepsilon)$ represents the higher-order small terms, which is negligible in calculation. Hence, Eq. (A.7) can be rewritten as:

$$a_{\mathrm{P}}^{\mathrm{B}^{v+}}\left(a_{\mathrm{P}}^{\mathrm{A}^-}\right)^v = a_{\mathrm{E}}^{\mathrm{B}^{v+}}\left(a_{\mathrm{E}}^{\mathrm{A}^-}\right)^v \tag{A.9}$$

where activities a_{E}^{i} and a_{P}^{i} can be written as $a_{\mathrm{E}}^{i} = \gamma_{\mathrm{E}}^{i} m_{\mathrm{E}}^{i}$ and $a_{\mathrm{P}}^{i} = \gamma_{\mathrm{P}}^{i} m_{\mathrm{P}}^{i}$, respectively, where $\gamma_{\mathrm{E/P}}^{i}$ is the activity coefficient, and $m_{\mathrm{E/P}}^{i}$ is the molar fraction,

$$m^i = \frac{c^i}{\sum c^{\alpha}} \tag{A.10}$$

where c^{α} is the molar concentrations of species α. It follows from Eq. (A.9) that

$$m_{\mathrm{P}}^{\mathrm{B}^{v+}}\left(m_{\mathrm{P}}^{\mathrm{A}^-}\right)^v = \gamma m_{\mathrm{E}}^{\mathrm{B}^{v+}}\left(m_{\mathrm{E}}^{\mathrm{A}^-}\right)^v \tag{A.11}$$

and $\gamma = \gamma_{\mathrm{E}}^{\mathrm{B}^{\nu+}}(\gamma_{\mathrm{E}}^{\mathrm{A}^-}/\gamma_{\mathrm{P}}^{\mathrm{A}^-})^{\nu}/\gamma_{\mathrm{P}}^{\mathrm{B}^{\nu+}}$, and $\gamma \geq 1$. In particular, $\gamma = 1$ for an ideal solution.

Π_{D} is determined using Eqs. (4) and (A.10). For an ideal dilute solution, $a_{\mathrm{E}}^{\mathrm{A}^-} \approx m_{\mathrm{E}}^{\mathrm{A}^-}$, $a_{\mathrm{P}}^{\mathrm{B}^{\nu+}} \approx m_{\mathrm{P}}^{\mathrm{B}^{\nu+}}$, $a_{\mathrm{E}}^{\mathrm{H_2O}} \approx 1 - m_{\mathrm{E}}^{\mathrm{A}^-} - m_{\mathrm{E}}^{\mathrm{B}^{\nu+}}$, $a_{\mathrm{P}}^{\mathrm{H_2O}} \approx 1 - m_{\mathrm{P}}^{\mathrm{A}^-} - m_{\mathrm{P}}^{\mathrm{B}^{\nu+}}$, Π_{D} can be computed as:

$$\Pi_{\mathrm{D}} = \frac{\mathrm{RT}\rho_{\oplus}^{\mathrm{H_2O}}}{\mathrm{M}^{\mathrm{H_2O}}} \ln\left(\frac{1 - m_{\mathrm{E}}^{\mathrm{A}^-} - m_{\mathrm{E}}^{\mathrm{B}^{\nu+}}}{1 - m_{\mathrm{P}}^{\mathrm{A}^-} - m_{\mathrm{P}}^{\mathrm{B}^{\nu+}}}\right) \tag{A.12}$$

Substituting Eq (A.10) in Eq. (A.12), one obtains

$$\Pi_{\mathrm{D}} = \frac{\mathrm{RT}\rho_{\oplus}^{\mathrm{H_2O}}}{\mathrm{M}^{\mathrm{H_2O}}} \left[\ln\left(1 - \frac{c_{\mathrm{E}}^{\mathrm{A}^-} + c_{\mathrm{E}}^{\mathrm{B}^{\nu+}}}{\sum c_{\mathrm{E}}^{\alpha}}\right) - \ln\left(1 - \frac{c_{\mathrm{P}}^{\mathrm{A}^-} + c_{\mathrm{P}}^{\mathrm{B}^{\nu+}}}{\sum c_{\mathrm{P}}^{\alpha}}\right)\right] \tag{A.13}$$

By Taylor's expansion and ignoring the higher-order small terms, Eq. (A.13) yields

$$\Pi_{\mathrm{D}} = \frac{RT\rho_{\oplus}^{\mathrm{H_2O}}}{\mathrm{M}^{\mathrm{H_2O}}} \left(\frac{c_{\mathrm{P}}^{\mathrm{B}^{\nu+}} + c_{\mathrm{P}}^{\mathrm{A}^-}}{\sum c_{\mathrm{P}}^{\alpha}} - \frac{c_{\mathrm{E}}^{\mathrm{B}^{\nu+}} + c_{\mathrm{E}}^{\mathrm{A}^-}}{\sum c_{\mathrm{E}}^{\alpha}}\right) \tag{A.14}$$

In the case of dilute solution, $\sum c_{\mathrm{P}}^{\alpha} \approx \sum c_{\mathrm{E}}^{\alpha} \approx c_{\mathrm{E/P}}^{\mathrm{H_2O}} \approx \rho_{\oplus}^{\mathrm{H_2O}}/\mathrm{M}^{\mathrm{H_2O}}$. Hence,

$$\Pi_{\mathrm{D}} \approx \mathrm{RT}\left(c_{\mathrm{P}}^{\mathrm{B}^{\nu+}} + c_{\mathrm{P}}^{\mathrm{A}^-} - c_{\mathrm{E}}^{\mathrm{B}^{\nu+}} - c_{\mathrm{E}}^{\mathrm{A}^-}\right) \tag{A.15}$$

Let c be the molar concentration (mol/L) of the equilibrium solution. The condition of electrical neutrality requires that

$$c_{\mathrm{E}}^{\mathrm{B}^{\nu+}} = \frac{c_{\mathrm{E}}^{\mathrm{A}^-}}{\nu} = c \tag{A.16}$$

$$\nu c_{\mathrm{P}}^{\mathrm{B}^{\nu+}} = c_{\mathrm{P}}^{\mathrm{A}^-} + \frac{c_{\mathrm{fix}}}{\phi} \tag{A.17}$$

where c_{fix} is the fixed negative charge density (mol/L), equal to the number of electrical charges per unit volume of soil, and given by

$$c_{\mathrm{fix}} = \frac{\mathrm{CEC} \cdot \rho_{\mathrm{d}}}{100} = \frac{\mathrm{CEC} \cdot \rho_{\mathrm{s}}}{100}(1 - \phi) \tag{A.18}$$

where CEC is the cation exchange capacity (meq/100 g or mmol/100 g); ρ_{d} is the dry density of soil (g/cm^3); ρ_{s} is the particle density of soil (g/cm^3) and equal to $\rho_w G_{\mathrm{s}}$, where G_{s} is the specific gravity of soil. Noticeably, not all the exchangeable cations contribute to the Donnan osmosis. Indeed, some exchangeable cations (say, those in the Stern layer) are strongly adsorbed onto clay particle surfaces, counterbalancing part of the negative charge of the clay minerals [11, 12, 35]. Hence, a reduction factor (δ) is introduced to obtain the effective fixed charge density ($c_{\mathrm{fix,e}}$) as

$$c_{\mathrm{fix,e}} = \delta c_{\mathrm{fix}} \tag{A.19}$$

Then, the electroneutrality condition in pore solution (Eq. (A.17)) can be rewritten as:

$$\nu c_{\mathrm{P}}^{\mathrm{B}^{\nu+}} = c_{\mathrm{P}}^{\mathrm{A}^-} + \frac{c_{\mathrm{fix,e}}}{\phi} \tag{A.20}$$

If c, c_{fix}, ν, and ϕ and δ are specified, $c_{\mathrm{P}}^{\mathrm{B}^{\nu+}}$ and $c_{\mathrm{P}}^{\mathrm{A}^-}$ can be obtained by simultaneously solving Eqs. (A.10)-(A.11), (A.16), and (A.18)-(A.20).

For NaCl solution, $\nu = 1$, and one can obtain

$$c_{\mathrm{P}}^{\mathrm{Na}^+} = \frac{\delta c_{\mathrm{fix}}}{2\phi}\left(\sqrt{1 + 4\left(\frac{\phi c}{\delta c_{\mathrm{fix}}}\right)^2} + 1\right) \tag{A.21}$$

$$c_{\mathrm{P}}^{\mathrm{Cl}^-} = \frac{\delta c_{\mathrm{fix}}}{2\phi}\left(\sqrt{1 + 4\left(\frac{\phi c}{\delta c_{\mathrm{fix}}}\right)^2} - 1\right) \tag{A.22}$$

Inserting Eqs. (A.21) and (A.22) into Eq. (A.15) yields

$$\Pi_{\mathrm{D}} = RT\left(\frac{\delta c_{\mathrm{fix}}}{\phi}\sqrt{1 + 4\left(\frac{\phi c}{\delta c_{\mathrm{fix}}}\right)^2} - 2c\right) \tag{A.23}$$

For $CaCl_2$ solution, $\nu = 2$, and one can obtain

$$\left(c_{\mathrm{P}}^{\mathrm{Cl}^-}\right)^3 + \frac{\delta c_{\mathrm{fix}}}{\phi}\left(c_{\mathrm{P}}^{\mathrm{Cl}^-}\right)^2 - 8c^3 = 0 \tag{A.24}$$

$$\Pi_{\mathrm{D}} = RT\left(\frac{3c_{\mathrm{P}}^{\mathrm{Cl}^-}}{2} + \frac{\delta c_{\mathrm{fix}}}{2\phi} - 3c\right) \tag{A.25}$$

Calculation of intergranular stresses σ_{v}'' during mechanical/chemical loading

Inserting Eqs. (2) and (4) into Eq. (1), one obtains

$$\sigma_{\mathrm{v}}'' = \sigma_{\mathrm{v}}' - \phi\Pi_{\mathrm{D}} + \phi_0\rho^l\Omega_0^l + \int_{\phi}^{\phi_0} \Pi_{\mathrm{D}}\mathrm{d}\phi \tag{A.26}$$

At the initial (reference) state, no vertical loading is applied (i.e., σ_{v0}'=0 kPa), and thus, the initial (reference) vertical intergranular stress is

$$\sigma_{\mathrm{v0}}'' = \phi_0\rho^l\Omega_0^l - \phi_0\Pi_{\mathrm{D0}} \tag{A.27}$$

which is the very initial effective stress keeping the soil intact. In the following calculations, σ_{v}'' represents $\sigma_{\mathrm{v}}'' - \sigma_{\mathrm{v0}}''$ for simplicity.

During a chemo-mechanical loading process, σ_{v}'' can be calculated stepwise. Assuming $\sigma_{\mathrm{vn-1}}''$(i.e., the value of σ_{v}'' at Step n-1) is known, and σ_{vn}'' can be determined as $\sigma_{\mathrm{vn}}'' = \sigma_{\mathrm{vn-1}}'' + \Delta\sigma_{\mathrm{vn}}''$. For mechanical loading, in which pore solution concentration remains practically constant (i.e., $\Delta c = 0$), where

$$\Delta\sigma_{\mathrm{vn}}'' = \Delta\sigma_{\mathrm{vn}}' - \phi_{\mathrm{n-1}} \cdot \Delta\Pi_{\mathrm{Dn}} \tag{A.28}$$

In the case of chemical loading, where $\Delta c \neq 0$ and $\Delta\phi \neq 0$,

$$\Delta\sigma''_{\mathrm{vn}} = \Delta\sigma'_{\mathrm{vn}} - \phi_{\mathrm{n-1}} \cdot \Delta\Pi_{\mathrm{Dn}} + \int_{\phi_{\mathrm{n-1}}}^{\phi_0} \frac{\partial \Pi_{\mathrm{D}}}{\partial c} \mathrm{d}\phi \cdot \Delta c_{\mathrm{n}} \tag{A.29}$$

Acknowledgements This research was funded by the Natural Science Foundation of China under Grants No. 51939011 and No. 41972290, and the Natural Science Foundation of Guangxi under Grant No. 2019GXNSFAA245025. All these financial supports are fully acknowledged.

References

1. Barbour SL, Fredlund DG (1989) Mechanisms of osmotic flow and volume change in clay soils. Can Geotech J 26(4):551–562
2. Bolt GH (1956) Physico-chemical analysis of the compressibility of pure clays. Géotechnique 6(2):86–93
3. Braggs B, Fornasiero D, Ralston J, Smart RS (1994) The effect of surface modification by an organosilane on the electrochemical properties of kaolinite. Clay Clay Miner 42(2):123–136
4. Chavali RVP, Ponnapureddy HPR (2018) Swelling and compressibility characteristics of bentonite and kaolin clay subjected to inorganic acid contamination. Int J Geotech Eng 12(5):500–506
5. Chen J, Anandarajah A, Inyang H (2000) Pore fluid properties and compressibility of kaolinite. J Geotech Geoenviron Eng 126(9):798–807
6. Di Maio C (1998) Discussion: 'Exposure of bentinite to salt solution: osmotic and mechnical effects.' Géotechnique 48(3):433–436
7. Di Maio C (2004) Consolidation, swelling and swelling pressure induced by exposure of clay soils to fluids different from the pore fluid. In: Loret B, Huyghe JM (eds) Chemo-mechanical couplings in porous media geomechanics and giomechanics. Springer, Vienna, pp 19–43
8. Di Miao C (1996) Exposure of bentonite to salt solution: osmotic and mechanical effects. Géotechnique 46(4):695–707
9. Di Miao C, Fenellif GB (1994) Residual strength of kaolin and bentonite: the influence of their constituent pore fluid. Géotechnique 44(2):217–226
10. Di Maio C, Santoli L, Schiavone P (2004) Volume change behaviour of clays: the influence of mineral composition, pore fluid composition and stress state. Mech Mater 36(5):435–451
11. Dominijanni A, Manassero M (2012) Modelling the swelling and osmotic properties of clay soils. Part II: The physical approach. Int J Eng Sci 51(1):51–73
12. Dominijanni A, Manassero M, Puma S (2013) Coupled chemical-hydraulic-mechanical behaviour of bentonites. Géotechnique 63(3):191–205
13. Gajo A, Maines M (2007) Mechanical effects of aqueous solutions of inorganic acids and bases on a natural active clay. Géotechnique 57(8):687–699
14. Gens A (2010) Soil-environment interactions in geotechnical engineering. Géotechnique 60(1):3–74
15. Gonçalvès J, Rousseau-Gueutin P, De Marsily G, Cosenza P, Violette S (2010) What is the significance of pore pressure in a saturated shale layer? Water Resour Res 46(4):W04514
16. Hang PT, Brindley GW (1970) Methylene blue absorption by clay minerals. Determination of surface areas and cation exchange capacities (clay-organic studies XVIII). Clay Clay Miner 18(4):203–212
17. Homand S, Shao JF (2000) Mechanical behaviour of a porous chalk and water/chalk interaction. Part I: experimental study. Oil Gas Sci Technol 55(6):591–598
18. Jang JB, Cao SC, Stern LA, Jung JW, Waite WF (2018) Impact of pore fluid chemistry on fine-grained sediment fabric and compressibility. J Geophys Res Solid Earth 123(7):5495–5514
19. Li ZZ, Katsumi T, Inui T, Takai A (2013) Fabric effect on hydraulic conductivity of kaolin under different chemical and biochemical conditions. Soils Found 53(5):680–691
20. Ma C, Eggleton RA (1999) Cation exchange capacity of kaolinite. Clay Clay Miner 47(2):174–180
21. Ma TT, Wei CF, Chen P, Li WT (2019) Chemo-mechanical coupling constitutive model for chalk considering chalk–fluid physicochemical interaction. Géotechnique 69(4):308–319
22. Ma TT, Yao CQ, Dong Y, Yi PP, Wei CF (2019) Physico-chemical approach to evaluating the swelling pressure of expansive soils. Appl Clay Sci 172:85–95
23. Mesri G, Olson RE (1971) Consolidation characteristics of montmorillonite. Géotechnique 21(4):341–352
24. Mitchell JK, Soga K (2005) Fundamentals of soil behavior, 3rd edn. Wiley, Hoboken
25. Moore R (1991) The chemical and mineralogical controls upon the residual strength of pure and natural clays. Géotechnique 41(1):35–47
26. Palomino AM, Santamarina JC (2005) Fabric map for kaolinite: effects of pH and ionic concentration on behavior. Clay Clay Miner 53(3):209–223
27. Rao SM, Thyagaraj T (2007) Swell–compression behaviour of compacted clays under chemical gradients. Can Geotech J 44(5):520–532
28. Sellin P, Leupin OX (2013) The use of clay as an engineered barrier in radioactive-waste management–a review. Clay Clay Miner 61(6):477–498
29. Shariatmadari N, Salami M, Karimpour FM (2011) Effect of inorganic salt solutions on some geotechnical properties of soil-bentonite mixtures as barriers. Int J Civ Eng 9(2):103–110
30. Sridharan A, Prakash K (1998) Characteristic water contents of a fine-grained soil-water system. Géotechnique 48(3):337–346
31. Sridharan A, Venkatappa Rao G (1973) Mechanisms controlling volume change of saturated clays and the role of the efiective stress concept. Géotechnique 23(3):359–382
32. Sridharan A, Venkatappa Rao G (1979) Shear strength behaviour of saturated clays and the role of the effective stress concept. Géotechnique 29(2):177–193
33. Sridharan A, Rao SM, Murthy NS (1988) Liquid limit of kaolinitic soils. Géotechnique 38(2):191–198
34. Thyagaraj T, Rao SM (2013) Osmotic swelling and osmotic consolidation behaviour of compacted expansive clay. Geotech Geol Eng 31(2):435–445
35. Tuttolomondo A, Ferrari A, Laloui L (2021) Generalized effective stress concept for saturated active clays. Can Geotech J 58:1627–1639
36. Wahid AS, Gajo A, Di Maggio R (2011) Chemo-mechanical effects in kaolinite. Part 1: prepared samples. Géotechnique 61(6):439–447
37. Wahid AS, Gajo A, Di Maggio R (2011) Chemo-mechanical effects in kaolinite. Part 2: exposed samples and chemical and phase analyses. Géotechnique 61(6):449–457
38. Wang YH, Siu WK (2006) Structure characteristics and mechanical properties of kaolinite soils. I. Surface charges and structural characterizations. Can Geotech J 43(6):587–600
39. Wang YH, Siu WK (2006) Structure characteristics and mechanical properties of kaolinite soils. II. Effects of structure on mechanical properties. Can Geotech J 43(6):601–617

40. Wei CF (2014) A theoretical framework for modeling the chemomechanical behavior of unsaturated soils. Vadose Zone J 13(9):1–21
41. Wen BP, Duzgoren-Aydin NS, Aydin A (2004) Geochemical characteristics of the slip zones of a landslide in granitic saprolite, Hong Kong: implications for their development and microenvironments. Environ Geol 47(1):140–154
42. Ye WM, Zhang F, Chen B, Chen YG, Wang Q, Cui YJ (2014) Effects of salt solutions on the hydro-mechanical behavior of compacted gmz01 bentonite. Environ Earth Sci 72(7):2621–2630
43. Yukselen Y, Kaya A (2008) Suitability of the methylene blue test for surface area, cation exchange capacity and swell potential determination of clayey soils. Eng Geol 102(1–2):38–45
44. Zhou JZ, Wei CF, Lai YM, Wei HZ, Tian HH (2018) Application of the generalized Clapeyron equation to freezing point depression and unfrozen water content. Water Resour Res 54(11):9412–9431